



Observed Budgets of Turbulence Kinetic Energy, Heat Flux, and Temperature Variance Under Convective and Stable Conditions

Alessandro E. D. Pozzobon¹ · Otávio C. Acevedo^{1,4} · Franciano S. Puhales¹ · Pablo E. S. Oliveira² · Rafael Maroneze³ · Felipe D. Costa³

Received: 22 October 2021 / Accepted: 4 February 2023 / Published online: 13 March 2023
© The Author(s), under exclusive licence to Springer Nature B.V. 2023

Abstract

The terms of the budget equations for turbulence kinetic energy (TKE), heat, flux, and temperature variance are evaluated observationally using 4 levels of turbulence observations made over a period of 10 months at a 30-m tower in southern Brazil. All terms are evaluated, except those associated with horizontal transport or pressure perturbations, which were not observed. The analysis is split between daytime, convective conditions and night-time, stable conditions. In both cases, the terms are initially shown in their original dimensional form as a function of the mean wind speed at 3 m, and the observations are then classified by net radiation. During the day, the TKE budget is dominated by shear and buoyant production, while dissipation is the main removal mechanism and the residual analysis indicates that the pressure transport term is positive near the surface. At night, the TKE budget is dominated by shear production and destruction by dissipation, while the buoyant destruction is about an order of magnitude smaller than both. The inferred role of pressure transport depends on the turbulence regime. In the daytime heat flux budget the dominant production mechanism varies between gradient and buoyant production, depending on mean wind speed and net radiation, while most of the destruction is mainly attributed to the pressure covariance term, inferred from the budget residual. At night, buoyancy becomes a relevant destruction mechanism, and its relationship with gradient production is related to the stable boundary layer turbulence regime. Temperature variance budget is a balance between gradient production and dissipation both at day and night, in which case the residual is larger and its possible causes are discussed. Dimensionless expressions for the dominant terms in the three budgets considered are compared to the data, as a function of the stability parameter.

Keywords Budgets · Heat flux · Second-order moments · Temperature variance · Turbulence kinetic energy

✉ Alessandro E. D. Pozzobon
alessandropozzobon@gmail.com

- ¹ Universidade Federal de Santa Maria (UFSM), Santa Maria, RS, Brazil
- ² Universidade Federal do Rio Grande do Norte (UFRN), Natal, RN, Brazil
- ³ Universidade Federal do Pampa (Unipampa), Alegrete, RS, Brazil
- ⁴ University of Oklahoma, Norman, OK, USA

1 Introduction

Turbulence is the most important feature of air flow in the planetary boundary layer (PBL), in fact defining it as a region different from the others in the atmosphere. Although it ultimately responds to processes at the lower and upper PBL limits, such as radiative exchange, molecular transfer of heat and entrainment exchange with the free-atmosphere, turbulence processes largely affect mean atmospheric variables in this portion of the atmosphere. Therefore, the adequate understanding and forecasting of quantities relevant to human activities, such as mean winds, mean temperature, and mean concentrations of gases cannot be attained unless there is knowledge on a variety of turbulence-related variables, such as the turbulent fluxes. Statistically, such fluxes are given by covariances between the quantity whose flux is being evaluated and components of the wind velocity. The physical processes that generate, destroy, and transport these and other second-order moments of turbulent perturbations of atmospheric variables are related in their budget equations. Their understanding is essential for the adequate representation of the turbulent processes in numerical models of the PBL, either through their parameterization or their solution through prognostic equations.

Mellor and Yamada (1974) proposed a hierarchy of turbulence closures for numerical weather forecast models of the PBL, based on the second-order moments that are solved prognostically, rather than parameterized. Of those they suggested, the most commonly employed approach is to solve only one second-order budget equation, that of turbulence kinetic energy (TKE). This variable is then employed to determine mixing lengths that compose the eddy diffusivities used to formulate the turbulent fluxes in terms of mean gradients (Weng and Taylor 2003; Cuxart et al. 2006; Steeneveld et al. 2006; Nakanishi and Niino 2009; Baas et al. 2018, among others). In the classification proposed by Mellor and Yamada (1974), the next level of complexity is achieved by additionally solving prognostic equations for the temperature variance $\overline{\theta'^2}$, and, in such case, the value of this variable is used as part of the stability function needed for eddy diffusivity determination (Nakanishi and Niino 2009) for estimating the counter-gradient contribution to the heat flux (Therry and Lacarrère 1983), or for both purposes (Kurbatskii and Kurbatskaia 2010). Complete second-order models where all fluxes and variances are solved prognostically have been implemented in some studies (Wilson 1988; Canuto et al. 1994; Cheng et al. 2002). Maroneze et al. (2019) have shown that the inclusion of a prognostic equation for the heat flux $\overline{w'\theta'}$, besides those for TKE, and $\overline{\theta'^2}$, specifically improves the solution of the turbulence regime in stable conditions. At the same time, a diversity of studies (Deardorff 1972; LeMone 1973; Salesky et al. 2017, among many others) indicates that in convective conditions the turbulence regime of forced or free convection is highly affected by the heat flux. For these reasons, the present study focuses on the budgets of TKE, $\overline{\theta'^2}$, and $\overline{w'\theta'}$. The first two are those whose prognostic equations are most commonly solved for employment in turbulence closure in PBL numerical schemes, while the third plays a crucial role in determining the PBL turbulence regime, in both convective and stable conditions.

The emphasis in these three second-order moments is also given in previous studies that have had a similar objective as the present one, that of evaluating the budgets of turbulence second-order moments in the PBL. The TKE budget is the most commonly addressed in observational studies. Its non-dimensionally scaled terms have been shown as a function of stability by Wyngaard and Coté (1971), Bradley et al. (1981), Frenzel and Vogel (1992), Li et al. (2008), among others. Its observations over surfaces have been made at forested (Meyers and Baldocchi 1991), urban (Christen et al. 2009; Nelson et al. 2011), marine (Edson and Fairall 1998; Sjoblom and Smedman 2002) and complex-terrain (Barman et al.

2019) environments. Observations of the vertical profiles of the TKE budget terms have been evaluated using aircraft data over land by Lenschow (1974), Pennell and LeMone (1974), Lenschow et al. (1980), and over the ocean by Chou et al. (1986), while Zhou et al. (1985) did so using tower data and Deardorff and Willis (1985) used laboratory observations. All these studies regard the daytime convective boundary layer (CBL) and are composed of a limited number of profiles. Modelling studies have also provided estimates of the vertical profiles of the TKE budget terms, both using Reynolds-averaged Navier—Stokes (RANS) equations (André et al. 1978; Therry and Lacerrère 1983), and large-eddy simulation (LES, Deardorff 1974; Moeng and Wyngaard 1989; Moeng and Sullivan 1994; Mironov et al. 2000). Of these studies, only André et al. (1978) also showed the profiles of the TKE budget terms at the nocturnal, stable boundary layer (SBL). More recently, these profiles have been presented in stable conditions using LES (Kosovic and Curry 2000) and direct numerical simulation (DNS), by Shah and Bou-Zeid (2014), Iman Gohari et al. (2017), Atoufi et al. (2019), and Lee et al. (2020). Of all these studies, a few also have shown the terms of the budgets of $\overline{w'\theta'}$, and $\overline{\theta'^2}$. These include their dependence on stability from observations for the $\overline{w'\theta'}$ budget (Wyngaard et al. 1971), for the $\overline{\theta'^2}$ budget (Wyngaard and Coté 1971; Edson and Fairall 1998), the vertical profiles of both budgets from observations (Chou et al. 1986), from RANS modelling (André et al. 1978), from LES (Moeng and Wyngaard 1989; Moeng and Sullivan 1994; Mironov et al. 2000), and from DNS under stable stratification (Shah and Bou-Zeid 2014). The vertical profiles of the $\overline{w'\theta'}$ budget terms above a canopy have been shown by Cava et al. (2006).

In the present study, the budgets of TKE, $\overline{w'\theta'}$ and $\overline{\theta'^2}$ are observationally determined using 10 months of turbulence data at 4 vertical levels over a pasture site in southern Brazil. The main difference from previous studies is the very long term of the observations, which reduce the effects of random variability in the averages. Besides, being at a subtropical location, where pre- and post-frontal conditions naturally succeed each other, horizontal transport terms are expected to average out over long periods, so that the budget residuals are more likely dominated by contributions from other terms not evaluated in the budgets, such as those associated with pressure perturbations. The budget terms are evaluated in terms of mean wind speed (in dimensional form) and stability (in dimensionless form), for both convective and stable conditions. In the analysis of the dimensional terms, the role of net radiation in controlling the second-order moments and their budgets is also considered.

The novelties of the study are:

- The evaluation of the budgets of TKE, heat flux and temperature variance for both convective and stable conditions using the same long dataset, which reaches broader limits of stability than previous studies;
- Presenting the budgets dimensionally, in terms of mean wind speed and its dependence on net radiation. This has been initially motivated by recent studies (Sun et al. 2012; van de Wiel et al. 2012) that found that in stable conditions the turbulence regime changes at a threshold wind speed, and the question whether such a transition may be influenced by the second-order budgets analyzed here. By evaluating the effects of near-surface mean wind speed and net radiation on the budgets, the present results may be useful to understand the controls exerted by these processes in turbulent quantities and to validate higher-order turbulence models in specific real world simulations;
- The long term of the observations offers more confidence for discarding horizontal advection by the mean wind and, therefore, a more robust inference of the budget residuals as being dominated by the not-observed terms associated with pressure perturbations;

- The dimensionless analysis over a broad range of the stability parameter offers indication of the stability limits over which the scaling used, based solely on local parameters, is valid.

In Sect. 2, the budget equations are presented, and the observations and their methods of analysis are described in Sect. 3. The results sections are separated by period in the day: CBL in Sect. 4 and SBL in Sect. 5. In both of them, first the equilibrium values of the three second-order moments are shown and described in terms of mean wind speed and net radiation, and later each of the three budgets are detailed with respect to the same quantities, dimensionally. In Sect. 6, the dimensionless budgets are shown for both convective and stable conditions. Conclusions appear in Sect. 7.

2 Budget Equations

The TKE budget considered in the present study is obtained by assuming horizontal homogeneity of turbulence and, therefore, neglecting the effects of horizontal flux convergence in both terms (*TT*) and (*PT*) of Eq. 1. Besides, in term (*SP*) the contributions from horizontal wind shear as $-\bar{u}^2 \partial \bar{u} / \partial x$ and $-\bar{u}' v' \partial \bar{u} / \partial y$ are neglected in comparison to those of the vertical wind shear, and the reference frame is rotated so that $\bar{v} = \bar{w} = 0$,

$$\frac{\partial e}{\partial t} = \underbrace{-\bar{u} \frac{\partial e}{\partial x}}_{(ADV)} - \underbrace{\overline{u' w'}}_{(SP)} \frac{\partial \bar{u}}{\partial z} + \frac{g}{\Theta_v} \overline{w' \theta'_v} - \frac{\partial \overline{w' e}}{\partial z} - \frac{1}{\bar{\rho}} \frac{\partial \overline{w' p'}}{\partial z} - \varepsilon. \tag{1}$$

$\left(\frac{BP}{D} \right)$
 (TT)
 (PT)
 (DIS)

In Eq. 1, u , v , and w are the wind velocity components, θ is potential temperature, p is air pressure, ρ is air density and g is gravity acceleration. Overbars represent averages over fixed time periods (see Sect. 3) and primes are instantaneous perturbations with respect to those averages. Therefore, e is TKE defined as half the sum of the variances of the wind velocities: $e \equiv 0.5(\overline{u'^2} + \overline{v'^2} + \overline{w'^2})$. Covariances $\overline{u' w'}$, $\overline{w' \theta'_v}$, $\overline{w' e}$ represent turbulent fluxes of momentum, buoyancy and TKE, respectively.

On the right-hand side (r.h.s) of Eq. 1, term *ADV* represents the advective transport by the mean wind and by eddies with temporal scale larger than the averaging time in each case (these combined contributions are generally referred as “advection” in the manuscript). *SP* is the shear TKE production, *BP/D* is the buoyant production (*BP* in convective conditions) or destruction (*BD* in stable conditions), *TT* is vertical TKE transport by turbulence, while *TP* is vertical TKE transport by pressure perturbations. Finally, *DIS* is the molecular dissipation of TKE.

In the present study, terms *SP*, *BP/D*, *TT* and *DIS* are directly observed by the turbulence observations carried out at the Santa Maria micrometeorological tower. Term *ADV* is neglected, based on the fact that it can be of either sign, depending on wind direction, so that it might nearly average out over a long time, such as the one used in the present analysis. The limitations of such an assumption are considered in the analysis. Term *PT* is not observed, as no observations of pressure perturbations are available, and its contribution to the equation residual, or the value necessary for TKE budget closure, is addressed in the results Sects. 4 and 5.

Equivalent assumptions to those made in Eq. 1 lead to the heat flux budget equation:

$$\frac{\partial \overline{w'\theta'}}{\partial t} = \underbrace{-\bar{u} \frac{\partial \overline{w'\theta'}}{\partial x}}_{(ADV)} - \underbrace{w'^2 \frac{\partial \bar{\theta}}{\partial z}}_{(GP)} + \underbrace{\frac{g}{\Theta_v} \overline{\theta'\theta'_v}}_{(BP/D)} - \underbrace{\frac{\partial \overline{w'^2\theta'}}{\partial z}}_{(TT)} - \underbrace{\frac{1}{\bar{\rho}} \frac{\partial \overline{\theta'\partial p'}}{\partial z}}_{(PC)}. \tag{2}$$

Given that the heat flux $\overline{W'\theta'}$ may be of either sign, we assume that any given term is regarded as a production term when it has the same sign of the existent heat flux, so that it contributes to the increase of its magnitude. Therefore, given that the heat flux is generally positive in daytime convective conditions and negative at night-time stable conditions, during the day positive terms represent production and negative terms represent destruction mechanisms, while the opposite occurs at night. In Eq. 2, *ADV* represents heat flux advection; *GP* is heat flux production by the thermal gradient; the buoyant term *BP/D* is always positive because $\theta' \approx \theta'_v$, so that the covariance between them approaches the variance of either one. Therefore, it represents production (*BP*) during the day when > 0 and destruction (*BD*) at night when < 0 ; *TT* is the heat flux transport by turbulence and *PC* is the pressure covariance term. Here, we are following studies such as Wyngaard et al. (1971) and Moeng and Wyngaard (1989) in presenting *PC* as a single term, but it is sometimes presented in two components as Shah and Bou-Zeid (2014),

$$-\frac{1}{\bar{\rho}} \frac{\partial \overline{\theta'\partial p'}}{\partial z} = -\frac{1}{\bar{\rho}} \frac{\partial \overline{p'\theta'}}{\partial z} + \frac{1}{\bar{\rho}} \frac{\partial \overline{p'\partial \theta'}}{\partial z},$$

where the first term on the right represents the heat flux transport by pressure perturbations and the second is the return-to-isotropy contribution. No molecular term is presented in Eq. 2 because they tend to be much smaller than the others in high Reynolds number turbulence when the molecular processes occur in scales in which turbulence is isotropic and, therefore, covariances between variables are negligible (Wyngaard et al. 1971).

Here, terms *GP*, *BP/D* and *TT* are directly observed. Term *ADV* is, to a first approximation, neglected assuming that advective effects tend to average out over a large period such as the one presently used. Term *PC* is not observed, and the possibility of assessing it as the residual necessary to produce budget closure (left-hand side zero in Eq. 2) is addressed in the results section.

Under similar assumptions of horizontal homogeneity and neglecting the horizontal thermal gradients with respect to the vertical ones in term *GP*, the budget of temperature variance $\overline{\theta'^2}$ is:

$$\frac{\partial \overline{\theta'^2}}{\partial t} = \underbrace{-\bar{u} \frac{\partial \overline{\theta'^2}}{\partial x}}_{(ADV)} - \underbrace{2\overline{w'\theta'}}_{(GP)} \frac{\partial \bar{\theta}}{\partial z} - \underbrace{\frac{\partial \overline{w'\theta'^2}}{\partial z}}_{(TT)} - \underbrace{\varepsilon_{\theta^2}}_{(DIS)} - \underbrace{\varepsilon_R}_{(RAD)}. \tag{3}$$

In Eq. 3, *ADV* is the advection, *GP* is $\overline{\theta'^2}$ production by the thermal gradient, *TT* is its transport by turbulence, *DIS* is the dissipation by molecular processes and *RAD* is the radiation destruction term. All terms, except for *ADV* and *RAD* are observed at the tower, being analyzed and discussed in Sects. 4 and 5.

3 Observations and Analysis

A 30-m micrometeorological tower has been operating at the campus of Universidade Federal de Santa Maria (UFSM) since 2013 (29° 43' 27.502'' S; 53° 45' 36.097'' W). In the present study, the period analyzed goes from 6 December 2019 to 31 October 2020, when 4 sonic anemometers operated, at heights of 3, 6, 14 and 30 m from the ground surface. The area is on a cattle-grazing experimental site covered by pasture. The tower is at a relatively lower portion of the terrain, with a few kilometres of fetch in the preferential wind-direction, which is to the south-east of the tower. A suburban environment starts at about 500 m to the north of the tower. Hills about 500-m high exist at about 5 km north of the tower. Further details on the site and measurements carried there, including pictures and the wind roses can be found at Rubert et al. (2018). The site roughness length (z_0) is 0.1 m when data from all wind directions are considered. Acevedo et al. (2021) have showed that z_0 varies with wind direction at the site, but given that in the present analysis no wind direction filtering is used, as a way of minimizing the effect of horizontal transport terms in the budgets, the value of 0.1 m must be considered.

The turbulence data used in the present study were measured at four different levels: 3, 6, 14 and 30 m above the ground. Fast response measurements of wind and sonic temperatures were performed with an Integrated Gas Analyzer and 3-D Sonic Anemometer (IRGASON, Campbell Scientific Inc.) at 3 m, CSAT3B 3-D sonic anemometer (Campbell Scientific Inc.) at 6 and 14 m, and a CSAT3 3-D sonic anemometer (Campbell Scientific Inc.) at 30 m, all sampled at 10 Hz. For the determination of temperature gradients, slow-response thermohygrometers installed at 4, 8 and 22 m have been used. Temperature has been measured using the CS215 temperature and relative humidity probe (Campbell Scientific Inc.) at 4 and 8 m, and using the HMP45C temperature and relative humidity probe (Campbell Scientific Inc.) at 22 m. The slow-response sensors have been intercompared prior to deployment, and the data have been corrected based on a linear adjustment following the intercomparison.

For the daytime convective case, data from 1000 to 1600 LST have been used, while night-time, stable data used went from 2200 to 0400 LST. The choice of only 6 h of data in each period has been made to assure that transitional periods have not been included in any time of the year. Turbulence statistics have been evaluated over 15-min periods at daytime, as previously done by Wyngaard et al. (1971) and Bradley et al. (1981), and 1-min periods at night-time, as used by Mahrt et al. (2013), Acevedo et al. (2016), and Stiperski et al. (2019), among others. These choices are a compromise to capture a large fraction of the turbulent contribution without including excessive low-frequency, non-turbulence influence in the statistics. In the terms that contain vertical gradients, those were evaluated as central finite differences between observations taken at the next level above and below the level under analysis. For this reason, the budget terms are shown only at levels 6 and 14 m, while values of the second-order budgets under consideration are shown at the 4 levels of observations.

Sonic temperatures have been used for temperature fluctuations. As they are a good approximation to virtual temperature (θ'_v) (Sjoblom and Smedman 2002), their covariances to vertical velocity fluctuations are a good approximation to the buoyancy flux, necessary in Eq. 1. On the other hand, it also means that all occurrences of θ' in the right side of Eqs. 2 and 3 are approached as $\theta' \approx \theta'_v$.

The TKE dissipation rate ε and temperature variance dissipation rate ε_{θ^2} have been determined from the second-order structure function for longitudinal velocity component (S_u^2) and for temperature (S_T^2), respectively, as done by Puhales et al. (2015). In general, the second-order structure function on the inertial sub-range can be written as $S_\alpha^2 = F_\alpha R^{2/3}$,

where r is the point separation distance and F_α is a function that depends on the second-order structure function nature. For the longitudinal wind speed $F_u = C_k \varepsilon^{2/3}$, where $C_k = 2.13$ is the Kolmogorov constant (Sreenivasan 1995). For temperature $F_T = C_T \varepsilon^{-1/3} \varepsilon_{\theta'}^2$ and $C_T = 3.2$ is defined under a constant skewness assumption (Kiely et al. 1996). As the second-order function is a power law on the inertial sub-range, a linear fit for 9 points on this particular range was employed to obtain ε and $\varepsilon_{\theta'}$ from the experimental data. The linear fit was performed using a moving window with 9 points across the second-order structure function domain. The window selected was one that provides a smallest deviation from the 2/3 exponent, with a coefficient of determination $R^2 \geq 0.8$. Data with an absolute error larger than 10% regarding the 2/3 exponent have been discarded.

The budget terms here analyzed are initially shown in a dimensional form, in terms of wind speed and net radiation. The majority of previous budget analysis has shown dimensionless forms of the terms, which is useful for providing a universal comparison of the terms among themselves at any given condition, as well as more easily allowing their use for modelling purposes (Wyngaard et al. 1971; Moeng and Wyngaard 1989; Sullivan and Moeng 1994, among others). However, the analysis of dimensionless budget terms masks the dependence of the budget itself in some of its controlling quantities. The analysis in terms of wind speed as a controlling variable has been motivated by the findings from studies such as those from Sun et al. (2012) and van de Wiel et al. (2012) that night-time turbulence regime is, to a great extent controlled by the mean wind speed. Here, the analysis is done in terms of the mean wind speed at 3 m, the lowest available in the observations. The wind speed near the surface is preferred to the one near the top of the tower because they maybe decoupled from each other, especially in very stable situations, in which case the budget variables near the surface are not related to the wind speed aloft. Although there is no knowledge that daytime turbulent quantities and regimes have an explicit dependence on mean wind speed, this is also considered as a control variable in the period, as a means of addressing to which extent such analysis is viable. In Sect. 6, stability is quantified in terms of the dimensionless parameter from Monin—Obukhov similarity theory, zL^{-1} at 3 m, where z is height above the ground and L is the Obukhov length, defined as $L = u_*^3 \Theta \left(\kappa g \overline{w'\theta'_v} \right)^{-1}$, where u_* is the friction velocity, defined as the squared root of the magnitude of the vertical flux of horizontal momentum, Θ is a reference temperature, κ is von Kármán constant, g is gravity acceleration and $\overline{w'\theta'_v}$ is the buoyancy flux.

All budgets are presented as bin averages, where the number of points in each bin is fixed. Therefore, each bin consists of n points of similar V , and their position in the horizontal axis is shown as the average V within the bin. The number n of points in each bin is 200 for convective conditions and 2000 in stable conditions, the difference coming from the fact that there are more observations in stable windows when the averaging window is smaller. For the temperature variance budget, n is 150 in convective and 1500 in stable conditions, because there are more missing points in this budget than in the others, arising from indeterminations in the temperature variance dissipation rate. Whenever any budget term was missing, the correspondent observation of all other terms of the same budget was not used.

4 Convective Case

Before addressing the budgets of the second-order moments, we look at how the near-surface values of TKE, heat flux and temperature variance depend on mean wind speed and net radiation (Fig. 1). At daytime, convective conditions, TKE increases near linearly with the

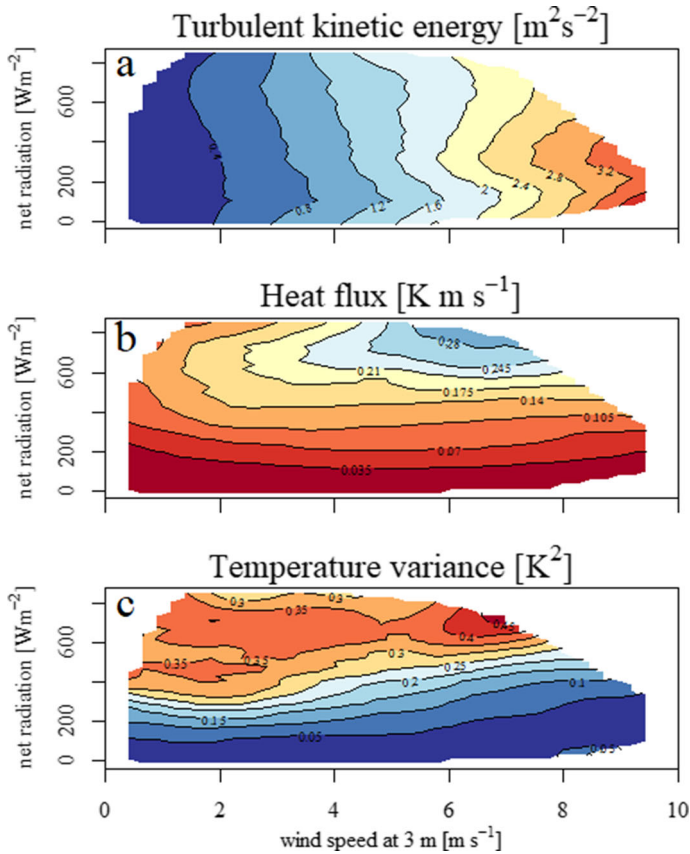


Fig. 1 Average daytime dependence of 3-m TKE (upper panels), 3-m heat flux (middle panels) and 3-m temperature variance (lower panels) on 3-m mean wind speed V and net radiation

near-surface mean wind speed from an average value near $0.5 \text{ m}^2 \text{ s}^{-2}$ for very weak wind speed to $2.5 \text{ m}^2 \text{ s}^{-2}$ for $V \cong 6 \text{ m s}^{-1}$ (Fig. 1a). For $V > 6 \text{ m s}^{-1}$, TKE is observed to increase more sharply with wind speed. In the entire range of wind speeds, TKE is only slightly affected by net radiation. In contrast with TKE, the heat flux (here approached by the buoyancy flux $w'\theta'_v$) is mostly dependent on net radiation, varying little with the mean wind speed, except for $R_n > 400 \text{ W m}^{-2}$ (Fig. 1b). Such a dependence on net radiation arises naturally from the role of the sensible heat flux as a major component of the surface energy budget. Interestingly, when $R_n > 400 \text{ W m}^{-2}$, the wind speed exerts an appreciable control on the heat flux. Given that the latent heat flux also increases slightly with wind speed in that net radiation range (not shown), this result implies lack of energy budget closure at low wind speeds. Similar to the heat flux, temperature variance (here approached by the sonic temperature variance $\overline{\theta'^2_v}$) is much more dependent on the net radiation than on the mean wind speed, and in this case it is regardless of the level of net radiation (Fig. 1c).

Based on these results, in the following analysis the second-order moment budgets are shown in terms of the mean wind speed, and the dominant terms are also shown by classes

of net radiation, to address if not only their magnitude, but also their dependence on wind speed is affected by R_n .

4.1 Turbulence Kinetic Energy Budget

In the daytime TKE budget (Eq. 1), SP increases nearly as the third power of the mean wind speed for all ranges of V (Fig. 2a). At 6 m, this is the dominant production term for $V > 1.5 \text{ m s}^{-1}$, but at 14 m this condition is restricted to $V > 2.5 \text{ m s}^{-1}$. BP dominates otherwise, and DIS is the main mechanism of TKE destruction, always exceeding TT , also negative at the entire extension of the tower (Fig. 2c), indicating that TKE is being transported by turbulence from the surface towards levels above the tower height. The residual term, necessary for budget closure is generally positive for all mean wind speeds. Such a residual must account for the role of pressure-transport term (TP), advection by the mean wind in all directions and horizontal TKE turbulent flux divergence, besides errors of any kind in the estimates. Given that horizontal transport terms by both the mean wind and turbulence are likely to average out over a large enough period at a location such as the site of the present study where pre- and post-frontal situations alternate sequentially, it is possible to speculate that most of the observed residual is caused by term TP . The residual found, of similar magnitude and

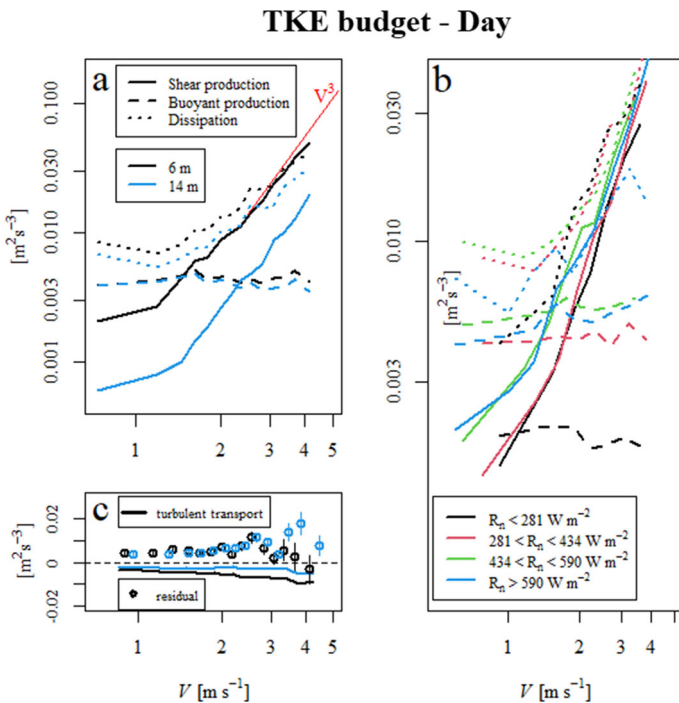


Fig. 2 Daytime dependence of the TKE budget terms (according to legend at panels a and c) on 3-m wind speed V (a and c). Terms that have a fixed sign are shown as their absolute values in a log scale at the panel a, while terms that may be of either sign are shown in a linear scale at panel c. Color relate to the vertical level, according to legend at panel a. Panel b shows the same terms as in panel a, classified in 4 classes of net radiation classes, according to legend. All classes have the same number of occurrences, representing a quartile of the total data

opposite sign to that of the other transport term, TT , gives confidence that such speculation may be at least approximately valid. This is because LES results indicate that TP has an opposite sign and the same order of magnitude than TT . Specifically, Moeng and Wyngaard (1989) have found, in a convective simulation with $-z_i L^{-1} \cong 15$, that near the surface TT is of opposite sign and nearly twice as large in magnitude than TP . A similar quantitative relationship has been found by the Deardorff and Willis (1985) laboratory study, where TP was inferred from the budget residual, and by Puhales et al. (2013) in a LES simulation of a diurnal cycle with $-z_i L^{-1}$ ranging between 7 and 15. In slightly more convective situations ($-z_i L^{-1}=18$), Moeng and Sullivan (1994) found the two transport terms to be of opposite signs and similar magnitudes near the surface.

Errors in each of the observed terms affect the errors in the residual estimates. Here, the errors are generally smaller because of the large number of observations in each averaged bin. We estimate the standard error SE of each of the terms evaluated as $SE_x = \sigma_x / \sqrt{n}$ where σ_x is the bin standard deviation and n is the number of observations in each bin (200 at daytime, 2000 at night-time). Here, it is important to notice that σ_x also contains naturally driven variability, due to differences in forcings, such as net radiation, within each bin. The accumulated residual error is given by the sum of the absolute values of the errors in each of the observed terms. The accumulated residual error is shown in Fig. 3c as vertical bars at each residual point. Despite incorporating errors in the 4 other terms, they are generally smaller than the estimated residuals and, except in large wind speeds, do not bring uncertainty to the sign of the residual, providing additional confidence in the association between the

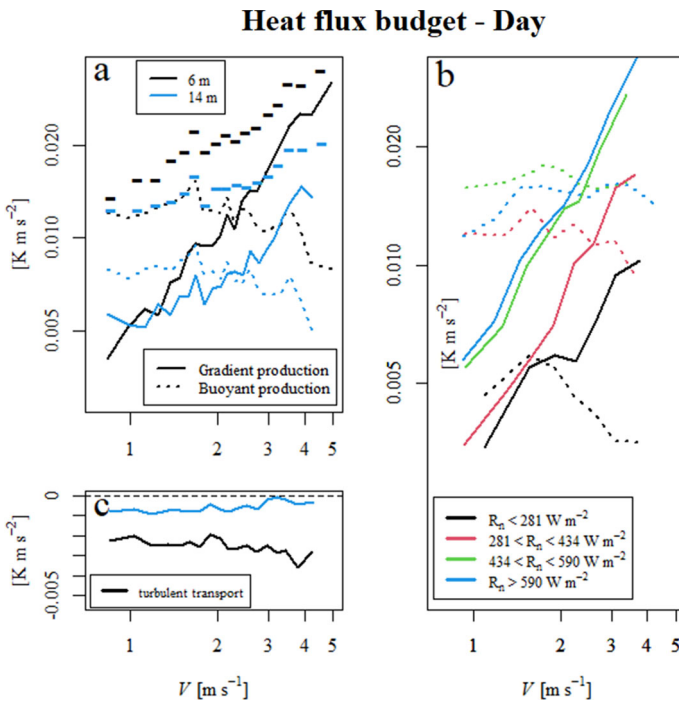


Fig. 3 The same as if Fig. 2, but for the heat flux budget. In this case, the residual is shown in panel a, and indicated by its sign in the logarithmic plot

residual observed and the role of the unobserved term associated with transport by pressure perturbations.

The dependence of SP , BP and DIS on mean wind speed is similar in all ranges of net radiation, although their magnitudes vary (Fig. 2b). The relative magnitude of the terms also depend on net radiation, so that BP increases more between the first and second quartiles of net radiation observations than over the next two classes, while the largest increase in SP occurs between the second and third quartiles. This is a consequence of the different effects net radiation has on the different budget terms, as suggested in Fig. 1, and it implies that the wind-speed threshold for budget dominance between SP and BP depends slightly on net radiation.

4.2 Heat Flux Budget

In the daytime heat flux budget (Eq. 2), our observations provide information on two production mechanisms, GP and BP , and the turbulent transport, TT (Fig. 3). When they are classified by the mean wind speed V at 3 m, it is observed that the dominant production mechanism changes at about $V = 2.5 \text{ m s}^{-1}$. For mean 3-m wind speed smaller than this threshold, BP is the dominant mechanism for $\overline{w'\theta'}$ production, while GP becomes dominant for $V > 2.5 \text{ m s}^{-1}$. This occurs mainly as a consequence of the increase of GP with the mean wind speed, as BP depends much less on this quantity. The large dependence of GP on V is caused by the role of the vertical velocity variance, which increases steadily with V , in this term. Term BP , on the other hand, depends mainly on the temperature variance $\overline{\theta'^2}$, which does not vary largely with V (Fig. 1c). Turbulence transports $\overline{w'\theta'}$ away from the surface, as TT is negative at both levels, and regardless of the wind speed (Fig. 3c), but the magnitude of this term is always smaller than either of the production mechanisms. The residual necessary for budget closure is, therefore, large and negative (Fig. 3a, “minus” signs). Such a residual is likely dominated by contributions from the PC term, although likely the other missing terms and errors of any kind also play a minor role. The role of PC as the dominant mechanism of $\overline{w'\theta'}$ suppression in the CBL has been established in the LES studies of Moeng and Wyngaard (1989), Moeng and Sullivan (1994) and Mironov et al. (2000).

The magnitude of both production terms varies largely with net radiation (Fig. 3b), but their dependence on mean wind speed is generally unaffected. As with the TKE budget (Fig. 2b), the terms vary differently with net radiation. Most of the variation of BP occurs between the first and second net radiation quartiles, while for GP it occurs between the second and third quartiles. Again, the consequence is that the mean wind speed threshold for budget dominance between GP and SP depends on R_n .

4.3 Temperature Variance Budget

The daytime $\overline{\theta'^2}$ budget (Eq. 3) is, to a large extent, a balance between production by GP and destruction by DIS (Fig. 4). The increase of GP with wind speed (Fig. 4a) is not driven by $\overline{w'\theta'}$, which varies much less with respect to that same variable (Fig. 1b). Therefore, the near twofold observed increase in GP from $V = 1 \text{ m s}^{-1}$ to $V = 3 \text{ m s}^{-1}$ is mostly driven by a similar increase in the thermal gradient with wind speed, which is unexpected, given that increased winds have a tendency to increase mixing, destroying vertical gradients. In the present case, it occurs mainly as a response to the daily cycle. The daytime thermal gradient near the surface is larger in the afternoon, when the surface is warmer, and this is also the time

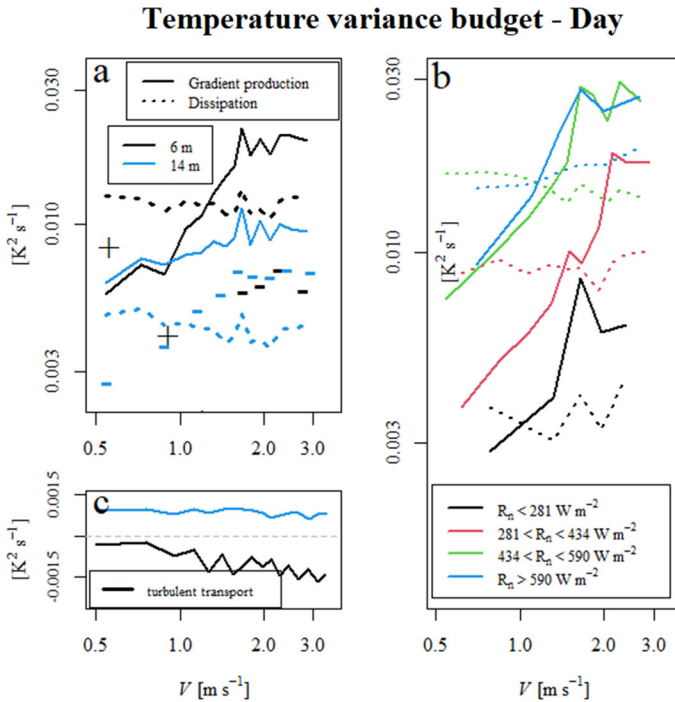


Fig. 4 The same as Fig. 2, but for the temperature variance budget. In this case, the residual is shown in panels a, and indicated by its sign in the logarithmic plot

when largest wind speed occurs, causing both variables to be positively correlated along the period of the analysis, with is between 1000 and 1600 local time. On the other hand, *DIS* is nearly independent of wind speed, being larger than *GP* for $V < 1.2 \text{ m s}^{-1}$, and smaller than *GP* otherwise, at 6 m. At 14 m, *GP* is always larger than *DIS*. *TT* is negative regardless of wind speed at 6 m, and positive at 14 m (Fig. 4b) indicating that the turbulent transport of $\overline{\theta'^2}$ operates over a shallow layer. Nevertheless, the magnitude of *TT* is much smaller than that of the other observed terms, so that the residual is nearly the difference between *GP* and *DIS*, at 6 m being negative for small wind speeds, positive for larger ones. Such a residual is smaller than the two dominant terms at 6 m, and it is likely composed of contributions of horizontal transport terms and observational errors of any kind. The average observed dependence of *GP* and *DIS* on mean wind speed persists over different ranges of net radiation, although the magnitude of each of the terms is observed to increase with R_n . (Fig. 4b).

5 Stable Case

At night, TKE generally increases with mean wind speed (Fig. 5a), as naturally expected. Contrasting with the daytime behaviour (Fig. 1a), there is some TKE dependence on net radiation, with larger TKE occurring with small than with large net radiative loss, for similar ranges of mean wind speed. The dependence of the nocturnal $\overline{w'\theta'_v}$ (Fig. 5b) mirrors the observations at daytime (Fig. 1b) in the sense that the heat flux depends almost exclusively

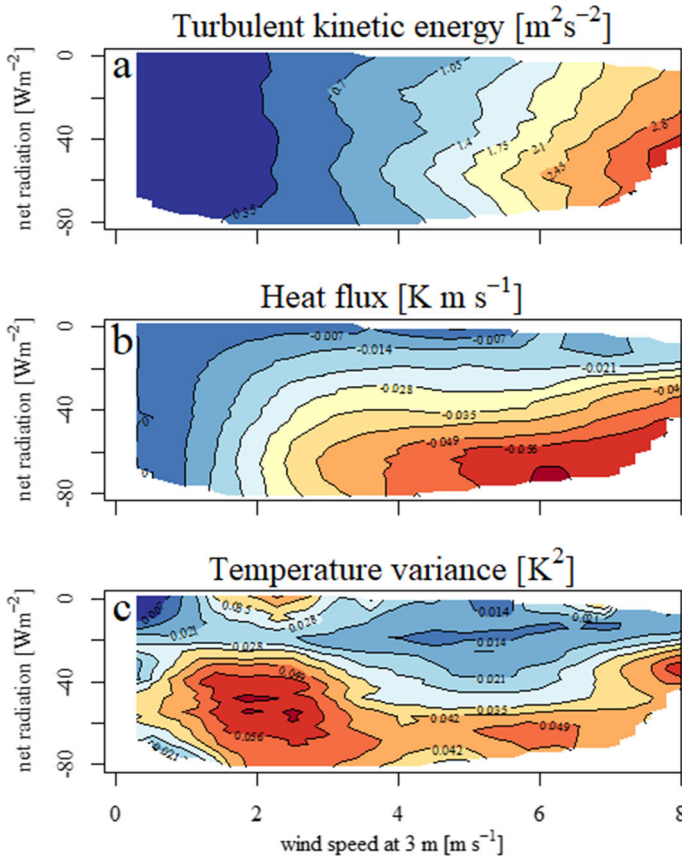


Fig. 5 The same as Fig. 1, but for the night-time period

on net radiation when the absolute value of R_n is small, and becomes also dependent on wind speed at larger values of $|R_n|$. A similar observation has been made by Acevedo et al. (2021), in terms of the 30-m mean wind speed. The range of wind speeds over which the heat flux increases with net radiation may be regarded as the weakly stable regime, when most of the energy lost by radiation is returned towards the surface by the heat flux. On the other hand, in the very stable regime, the heat flux is unable to provide such an energy return, and as a consequence heat flux and net radiation are less dependent of each other. The temperature variance $\overline{\theta_v^2}$ peaks at $V \cong 2 \text{ m s}^{-1}$ for most ranges of net radiation (Fig. 5c). In fact, the maximum $\overline{\theta_v^2}$ in Fig. 5c generally occur at mean wind speeds that coincide with those when the heat flux quits depending on mean wind speed and becomes solely dependent on net radiation, in Fig. 5b. It means that $\overline{\theta_v^2}$ tends to be maximum at the SBL regimetransition, a result in agreement with those found by Acevedo et al. (2016). Besides, there is a clear tendency of larger values of $\overline{\theta_v^2}$ to occur when the radiative loss is larger, a behaviour that also mirrors the daytime observations (Fig. 1c).

5.1 Turbulence Kinetic Energy Budget

In terms of magnitude, the two dominant terms of the TKE budget (Eq. 1) in stable conditions are *SP* and *DIS* (Fig. 6a). *SP* is larger than *DIS* at large *V*, which is the weakly stable regime. In the limit of large *V*, the ratio $DIS SP^{-1}$ is minimum, approaching 0.7, meaning that at night-time at least 70% of the turbulence produced by the wind shear is molecularly dissipated. This is similar to the ratio between these two terms found in the weakly stable LES of Kosovic and Curry (2000). In the very stable regime, on the other hand, at small *V* there is an excess of *DIS* over *SP*, implying that other TKE production mechanisms are present (van Hooijdonk et al. 2015). Despite the dominant role played by *BD* in driving the SBL regime transition (Bou-Zeid et al. 2018; Maroneze et al. 2019), *DIS* is always the largest term amongst the sink mechanisms. *BD* increases with *V*, as all terms do, but its relative contribution as a sink is larger in the very stable ($BD DIS^{-1} \cong 0.23$ at small *V*) than in the weakly stable regime ($BD DIS^{-1} \cong 0.05$ at large *V*), as previously shown by Acevedo et al. (2016). The *TT* term is small in magnitude (Fig. 6c). At $V > 2.0 \text{ m s}^{-1}$, *TT* is negative at 6 m and positive at 14 m, implying TKE turbulent transport from the lower to upper levels over a shallow layer that is covered by the tower extension. The magnitude of the TKE loss near the surface by *TT* in these situations is of the same order of magnitude as that provided by the *BD* term. For $V < 2.0 \text{ m s}^{-1}$, on the other hand, *TT* is positive both at 6 and 14 m, as may be expected, given that in such very stable regime TKE increases with height, as shown in Fig. 6a, therefore being transported downward.

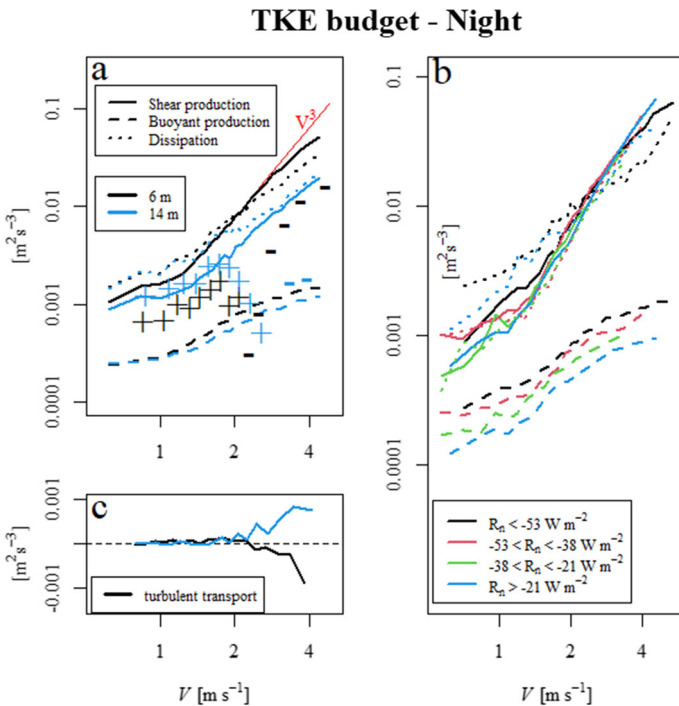


Fig. 6 The same as Fig. 2, but for the night-time TKE budget. In this case, the residual is shown in panels a, and indicated by its sign in the logarithmic plot

As a consequence of all these observed patterns of SP , DIS , BD and TT , the residual necessary for TKE budget closure is positive for small V , and negative otherwise, being mainly determined by the balance between the dominant terms SP and DIS . It is unclear the extent to which such a residual found indicates that the PT term is positive under very stable and negative under weakly stable conditions near the surface, especially because at night it is more likely that unaccounted horizontal transport terms by mean winds and turbulence are relevant. Acevedo et al. (2016) also found a dominance of DIS over SP that implies a positive residual in very stable conditions. The same was observed by Smeets et al. (1998) for $zL^{-1} > 0.3$, who suggested that PT must be positive in that range of stabilities to provide budget closure. Kosovic and Curry (2000) presented the vertical profiles of the TKE budget terms during a weakly stable simulation, finding negative PT near the surface. Cuxart et al. (2002) describe observations of PT along a night with intermittent turbulence, finding it to be generally negative near the surface and positive above 30 m. Therefore, the TKE budget residual from the present analysis indicates that PT is positive near the surface in very stable conditions, in agreement with Smeets et al. (1998) and with Acevedo et al. (2016), and negative in weakly stable conditions in agreement with the LES of Kosovic and Curry (2000). Nevertheless, there are large uncertainties associated with undetermined terms in the budget and errors of any kind, which imply that such a result must be accepted with caution. Being mostly driven by the heat flux, the magnitude of BD varies consistently with net radiation, being larger when the radiative loss is reduced (Fig. 6b). TKE dissipation rate is enhanced in the class of largest radiative loss for very weak winds. Given that in such case DIS exceeds SP , it is clear that additional TKE sources exist, which could be the horizontal transport by enhanced low-frequency submeso activity under these conditions.

5.2 Heat Flux Budget

In stable conditions, the buoyant term is positive and, therefore, opposes the downward heat flux, being regarded here as a destruction mechanism. The budget is, therefore, dominated by GP and BD , which oppose each other (Fig. 7). At large V , GP exceeds BD , while the opposite occurs at small V . Similar behaviour in terms of the mean wind speed has been found by Acevedo et al. (2016), who also found that the dominance between the two terms near the surface switched with the SBL regime: in the very stable case $|BD| > GP$, while $|BD| < GP$ in the weakly stable regime. The same occurs at the Santa Maria data set, where both terms are equal at $V \cong 1.2 \text{ m s}^{-1}$ (Fig. 7a), but this threshold also depends on net radiation (Fig. 7b). Therefore, the present results indicate that the heat flux budget and the condition $|BD|GP^{-1} = 1$ may be a good objective indicator of the SBL regime transition, as found by Acevedo et al. (2016). The residual necessary for budget closure is negative (and, therefore, contributing to the existing negative heat flux) with small V , when $|BD| > GP$ and positive (“destroying” heat flux) in the opposite case, when $|BD| < GP$. As in the convective case, it is likely that such a residual is dominated by PC , so that the present results offer a hint on how such a term behaves in stable conditions. It cannot be compared to estimates of this term from LES, as there are no such studies of the heat flux budget in stable conditions. The DNS study of Shah and Bou-Zeid (2014) made that analysis for Reynolds number ranging from 400 to 900. They divided the contribution of the PC term to the heat flux budget into a transport and a return-to-isotropy term, finding that both had opposing signs (negative transport, positive return-to-isotropy) and similar magnitudes near the surface, so that the total contribution to the heat flux budget is small. In that case, this result combined with those shown in Fig. 7a, b, allows speculating that when V is large, the

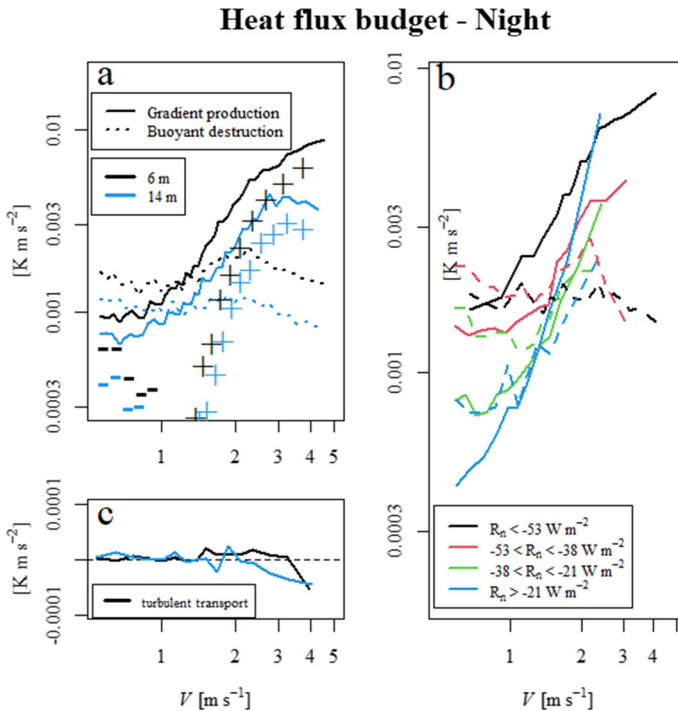


Fig. 7 The same as Fig. 2, but for the night-time heat flux budget. In this case, the residual is shown in panels a, and indicated by its sign in the logarithmic plot

negative residual is dominated by the transport portion of the term in the heat flux budget. On the other hand, when V is small, PC is likely dominated by the positive contributions from the return-to-isotropy component of this term.

5.3 Temperature Variance Budget

The temperature variance budget is dominated by GP , regardless of wind speed and height (Fig. 8). The most important destruction mechanism observed is DIS , while TT , transfers $\overline{\theta'^2}$ away from the surface at 6 m. Nevertheless, both of them together account for less than half of the production by GP , so that a large negative residual is necessary to close the budget at 6 m. At 14 m, GP has decreased relatively more than DIS and, therefore, the residual is smaller than DIS , despite TT being almost negligible. The largest values of GP occur either with very small V , when the thermal gradient is usually large, or with very large V , when fluxes are still large (Fig. 5b) and the thermal gradient has not been totally destroyed. Nevertheless, the combined effects of thermal gradient and $\overline{w'\theta'}$ cause GP to not vary largely with V (Fig. 8a) On the other hand, a larger dependence on V is observed in both DIS and TT (Fig. 9c), which increase with V The magnitude of both GP and DIS increase appreciably with the net radiative loss (Fig. 8b), but their overall dependence on wind speed follows what is observed in the average (Fig. 8a).

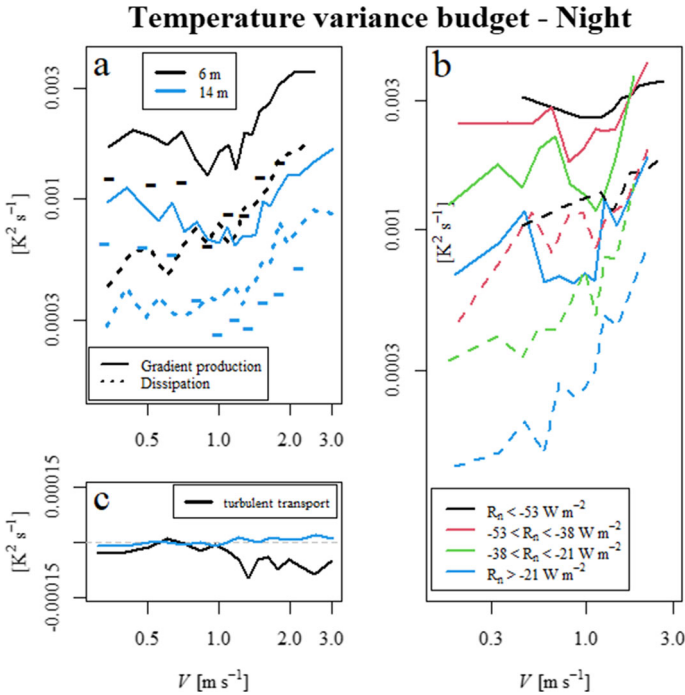


Fig. 8 The same as Fig. 2, but for the night-time temperature variance budget. In this case, the residual is shown in panels a, and indicated by its sign in the logarithmic plot

Given that the only terms not observed in the $\overline{\theta'^2}$ budget are those associated with radiative processes and with the horizontal transport, both by the mean wind and by turbulence, the large residual found suggest that either these terms are important or that the errors in the estimate are large. Dias and Brutsaert (1998) suggested that term *RAD* plays a small role in the $\overline{\theta'^2}$ budget at the stable surface layer (Eq. 3). At the same time, although the long-term observations in the present study and the much better closure of the budgets of TKE and $w'\theta'$ presented in the previous sections might suggest that the horizontal transport terms should also be small, it is possible that such contributions are enhanced in the $\overline{\theta'^2}$ budget, as small horizontal temperature contrasts may produce scalar variance. In any case, it is likely that one of those processes is playing an unexpected role. It is also somewhat surprising that *DIS* is so much smaller than *GP*, contrasting with the observations at daytime, when these terms have comparable magnitudes (Fig. 4), and with the results from the DNS by Shah and Bou-Zeid (2014), who found $|DIS| > GP$ and $TT > 0$ near the surface.

6 Dimensionless Budgets

To properly compare the present results to those from previous studies that analyzed the second-order budgets, in this section they are shown in dimensionless form. This is done only for the 6-m level, for simplicity, and the results are presented in Fig. 9. The TKE budget terms, when scaled by $u_*^3(\kappa z)^{-1}$ (Fig. 9a, b) are generally well represented by classical similarity

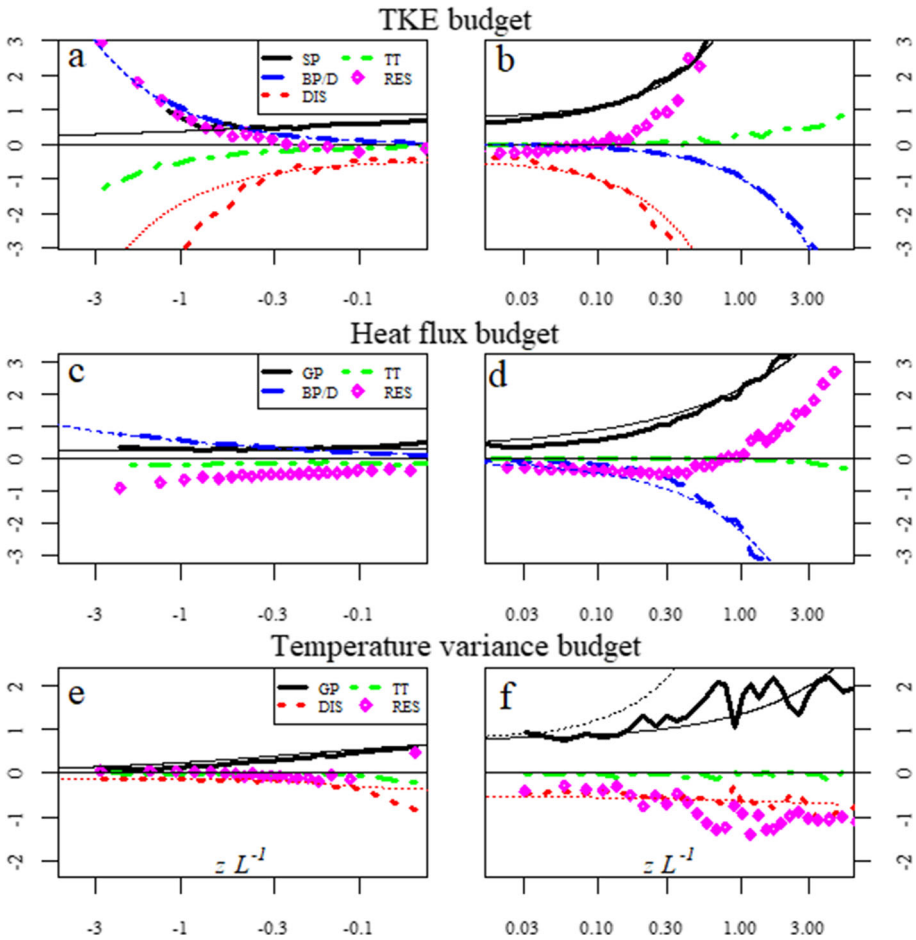


Fig. 9 Dimensionless budgets of turbulence kinetic energy (upper panels), heat flux (middle panels) and temperature variance (lower panels), for convective (left panels) and stable conditions (right panels), at 6 m. In each budget, the terms are shown as thick lines, identified by the legend at the left panel, and they are identified by the letters assigned to them in Eqs. 1–3. In all panels, thin lines indicate mathematical expressions, described in the text

relationships. The most important difference is that $SPu_*^{-3}(\kappa z)$, which is often represented as the dimensionless wind shear Φ_M , does not approach unity at the neutral limit of $zL^{-1} \rightarrow 0$, but 0.75. Reductions of the neutral value of Φ_M have been described by Garratt (1980), who attributed them to wake generation by a vegetated surface. The expressions proposed by Wyngaard et al. (1971) for Φ_M corrected by a multiplying factor of 0.75 (Table 1) provide a fairly good adjustment to the observations of the present study (Fig. 9a, b, thin black lines) for the entire range of zL^{-1} values in the stable side, and for $|zL^{-1}| > 0.5$ in the convective side. These results, therefore, indicate that beyond this limit of instability convective scaling may be more appropriate than surface-based Monin—Obukhov similarity, for this dataset. This conclusion is supported by the dimensionless dissipation rate $DISu_*^{-3}(\kappa z) \equiv \Phi_\epsilon$, which is well-represented over a similar range of zL^{-1} by the expression proposed by Albertson et al. (1997), again multiplied by a factor of 0.75 (Fig. 9a, thin dotted red line). Under stable

Table 1 Algebraic expressions used to represent the second-order budget terms in Fig. 9

Term	Budget equation	Condition	Dimensionless expression	Adjustment	Reference on which is based
SP	TKE	$zL^{-1} < 0$	$\frac{\partial \bar{u}}{\partial z} \frac{\kappa z}{u_*}$	$0.75(1 - 15 \frac{z}{L})^{-1/4}$	Wyngaard et al. (1971)
SP	TKE	$zL^{-1} > 0$	$\frac{\partial \bar{u}}{\partial z} \frac{\kappa z}{u_*}$	$0.75(1 + 4.7 \frac{z}{L})$	Wyngaard et al. (1971)
DIS	TKE	$zL^{-1} < 0$	$-\frac{\epsilon \kappa z}{u_*^3}$	$-(0.46 - 2.78 \frac{z}{L})$	Albertson et al. (1997)
DIS	TKE	$zL^{-1} > 0$	$-\frac{\epsilon \kappa z}{u_*^3}$	$-(0.46 + 5.6 \frac{z}{L})$	Wyngaard (1973)
GP	$\overline{w'\theta'}$	$zL^{-1} < 0$	$-\frac{\kappa z w'^2}{u_* w'\theta'} \frac{\partial \bar{\theta}}{\partial z}$	$0.28 - 0.17(-\frac{z}{L})^{2/3}$	-
GP	$\overline{w'\theta'}$	$zL^{-1} > 0$	$-\frac{\kappa z w'^2}{u_* w'\theta'} \frac{\partial \bar{\theta}}{\partial z}$	$0.28 + 1.88(\frac{z}{L})^{1/2}$	-
BP	$\overline{w'\theta'}$	$zL^{-1} < 0$	$\frac{\kappa z g}{\Theta_v} \frac{\overline{\theta'\theta'_v}}{u_* w'\theta'}$	$0.54(-\frac{z}{L})^{2/5}$	-
BD	$\overline{w'\theta'}$	$zL^{-1} > 0$	$\frac{\kappa z g}{\Theta_v} \frac{\overline{\theta'\theta'_v}}{u_* w'\theta'}$	$-[1.1(\frac{z}{L})^{1/2} - 1.2\frac{z}{L} + 0.027(\frac{z}{L})^2]$	-
GP	$\overline{\theta'^2}$	$zL^{-1} < 0$	$-\frac{2\kappa z u_*}{w'\theta'} \frac{\partial \bar{\theta}}{\partial z}$	$0.74(1 - 9 \frac{z}{L})^{-1/2}$	Wyngaard and Coté (1971)
GP	$\overline{\theta'^2}$	$zL^{-1} > 0$	$-\frac{2\kappa z u_*}{w'\theta'} \frac{\partial \bar{\theta}}{\partial z}$	$0.74 + 0.6(\frac{z}{L})^{2/3}$	-
DIS	$\overline{\theta'^2}$	$zL^{-1} < 0$	$-\frac{\kappa z u_* \epsilon}{(w'\theta')^2}$	$-\frac{0.58}{(1+e^{-9.3 \frac{z}{L}})} + 0.14$	-
DIS	$\overline{\theta'^2}$	$zL^{-1} > 0$	$-\frac{\kappa z u_* \epsilon}{(w'\theta')^2}$	$-[0.43 + 0.2(\frac{z}{L})^{1/5}]$	-

stratification, the suggestion from Wyngaard (1973) of a linear relationship between Φ_ϵ and zL^{-1} provides a good description of the observed dissipation rates, with the coefficients shown in Table 1. The dimensionless buoyant term of the TKE budget is mathematically identical to zL^{-1} .

In the heat flux budget, terms have been scaled by $u_* \overline{w'\theta'} (\kappa z)^{-1}$. Because the heat flux appears in the scaling, positive (negative) dimensionless terms represent gain (loss), regardless of the flux sign. The dimensionless heat flux budgets found present two substantial differences from the results of Wyngaard et al. (1971). The first is a change in dominance in convective conditions, at $zL^{-1} \approx -0.2$, absent in Wyngaard et al. (1971), who found that GP and BP converge to a similar value at the free convection limit of large $-zL^{-1}$ (Fig. 9c). Here, BP clearly dominates over GP in these conditions, while the opposite occurs

at the neutral limit of $zL^{-1} \rightarrow 0$. The second difference regards the residual term in stable conditions. While Wyngaard et al. (1971) found it to be always negative when $zL^{-1} > 0$, the present results indicate that the budget residual switches sign at $zL^{-1} \approx 0.7$ (Fig. 9d). This is a consequence of GP being always larger than the magnitude of BD in their results, while here $|BD| > GP$ in very stable conditions, as confirmed by Acevedo et al. (2016). Therefore, if the residual is assumed to be dominated by the pressure transport term PC , the present results indicate that PC is the dominant heat flux loss mechanism in all conditions, except for very stable ones, when BD plays that role. Algebraic expressions that adjust the GP and BP/D terms in terms of the stability parameter zL^{-1} in convective and stable conditions are presented in Table 1, and shown by thin lines in Fig. 9c, d.

The temperature variance budget terms have been scaled by $(\overline{w'\theta'})^2 (u_* \kappa z)^{-1}$, being shown in Fig. 9e, f. In convective conditions, the dimensionless GP term is well represented by the expression proposed by Wyngaard and Coté (1971), and presented at Table 1 (Fig. 9a, thin black line). In stable conditions, on the other hand, the proposition by Wyngaard and Coté (Fig. 9f, thin dotted black line) fails to reproduce the observed behaviour, and an alternative expression is given in Table 1, and shown as a thin solid black line in Fig. 9f. Algebraic expressions for the dimensionless temperature variance dissipation rate are also suggested in Table 1, based on the data from the present study.

7 Conclusion

The main contribution of the present study is a long-term analysis, which allowed detailed observations of the dependence of the budget terms on the mean wind speed, net radiation and stability, here represented by the stability parameter zL^{-1} . With such a dataset available, it aimed on answering the two following research questions: -How do the budgets of turbulent kinetic energy (TKE), heat flux ($\overline{w'\theta'}$) and temperature variance ($\overline{\theta'^2}$) depend on the mean wind speed and net radiation in both daytime and night-time conditions? How much are the results from previous observations, typically obtained in short-term campaigns supported by this longer dataset?

Regarding the first question, the budget analysis in terms of wind speed (V) and net radiation has established that amongst the three second-order moments considered, TKE is mostly controlled by the wind speed, with little dependence on net radiation, while the opposite occurs for $\overline{\theta'^2}$. The heat flux, on the other hand, has a mixed dependence: both at day and night, it is only controlled by V when the absolute value of R_n is large. Wind speeds at which there is a switch in the term that dominates the budget has been found in many cases. During daytime, TKE production is dominated by the buoyant term for low wind speeds and by the shear term for large wind speeds, while heat flux production is dominated by the buoyant term in low wind speeds and by the thermal gradient term for large wind speeds. At night, the magnitude of heat flux production by the thermal gradient only exceeds that of buoyant destruction when a wind speed threshold is exceeded. In all cases, the wind speed thresholds under which budget dominance changes is dependent on net radiation.

For the second question, in general previous results are supported by the present analysis, with some novelties. A particularly interesting piece of evidence refers to effects of pressure transport terms, although it is based on residual analysis. Results indicate that the pressure transport term in the TKE budget opposes the turbulent transport term in convective conditions, but is smaller in magnitude. In stable conditions, the uncertainty is bigger, but the

present results point to a negative role of the transport term by pressure perturbations in the weakly stable regime, that becomes positive in the very stable regime. Given that the two transport terms are often parameterized as a single one in models that solve the TKE budget equation (Duykerke 1988; Nakanishi and Niino 2009; Han and Bretherton 2019), this is an important finding that may help improving such parameterizations.

Acknowledgements This study has been supported by Brazilian research agencies Comissão de Aperfeiçoamento de Pessoal de Ensino Superior (CAPES), and Conselho Nacional de Desenvolvimento Científico e Tecnológico (CNPq), through grants 307024/2017-2 and 428015/2016-6. The authors thank Dr. Margaret LeMone and two anonymous reviewers for useful suggestions during the reviewing process.

References

- Acevedo OC, Mahrt L, Puhales FS, Costa FD, Medeiros LE, Degrazia GA (2016) Contrasting structures of the decoupled and coupled states of the stable boundary layer. *Q J R Meteorol Soc* 142(695):693–702. <https://doi.org/10.1002/qj.2693>
- Acevedo OC, Costa FD, Maroneze R, Carvalho AD Jr, Puhales FS, Oliveira PE (2021) External controls on the transition between stable boundary layer turbulence regimes. *Q J R Meteorol Soc* 147(737):2335–2351. <https://doi.org/10.1002/qj.4027>
- Albertson JD, Parlange MB, Kiehl G, Eichinger WE (1997) The average dissipation rate of turbulent kinetic energy in the neutral and unstable atmospheric surface layer. *J Geophys Res Atmos* 102(D12):13423–13432. <https://doi.org/10.1029/96JD03346>
- André J, De Moor G, Lacarrere P, Du Vachat R (1978) Modeling the 24-hour evolution of the mean and turbulent structures of the planetary boundary layer. *J Atmos Sci* 35(10):1861–1883. [https://doi.org/10.1175/1520-0469\(1978\)035%3C1861:MTHEOT%3E2.0.CO;2](https://doi.org/10.1175/1520-0469(1978)035%3C1861:MTHEOT%3E2.0.CO;2)
- Atoufi A, Scott KA, Waite ML (2019) Wall turbulence response to surface cooling and formation of strongly stable stratified boundary layers. *Phys Fluids* 31:085114. <https://doi.org/10.1063/1.5109797>
- Baas P, van de Wiel BJH, Van der Linden SJA, Bosveld FC (2018) From near-neutral to strongly stratified: adequately modelling the clear-sky nocturnal boundary layer at Cabauw. *Boundary-Layer Meteorol* 166(2):217–238. <https://doi.org/10.1007/s10546-017-0304-8>
- Barman N, Borgohain A, Kundu SS, Roy R, Saha B, Solanki R, Kiran Kumar MVP, Raju PLN (2019) Daytime temporal variation of surface-layer parameters and turbulence kinetic energy budget in topographically complex terrain around Umiam, India. *Boundary-Layer Meteorol* 172(1):149–166. <https://doi.org/10.1007/s10546-019-00443-6>
- Bou-Zeid E, Gao X, Ansonce C, Katul GG (2018) On the role of return to isotropy in wall-bounded turbulent flows with buoyancy. *J Fluid Mech* 856:61–78. <https://doi.org/10.1017/jfm.2018.693>
- Bradley EF, Antonia RA, Chambers AJ (1981) Turbulence Reynolds number and the turbulent kinetic energy balance in the atmospheric surface layer. *Boundary-Layer Meteorol* 21:183–197. <https://doi.org/10.1007/BF02033936>
- Canuto VM, Minotti F, Ronchi C, Ypma RM, Zeman O (1994) Second-order closure PBL model with new third-order moments: comparison with LES data. *J Atmos Sci* 51(12):1605–1618. [https://doi.org/10.1175/1520-0469\(1994\)051%3C1605:SOCPMW%3E2.0.CO;2](https://doi.org/10.1175/1520-0469(1994)051%3C1605:SOCPMW%3E2.0.CO;2)
- Cava D, Katul GG, Scrimieri A, Poggi D, Cescatti A, Giostra U (2006) Buoyancy and the sensible heat flux budget within dense canopies. *Boundary-Layer Meteorol* 118:217–240. <https://doi.org/10.1007/s10546-005-4736-1>
- Cheng Y, Canuto VM, Howard AM (2002) An improved model for the turbulent PBL. *J Atmos Sci* 59(9):1550–1565. [https://doi.org/10.1175/1520-0469\(2002\)059%3C1550:AIMFTT%3E2.0.CO;2](https://doi.org/10.1175/1520-0469(2002)059%3C1550:AIMFTT%3E2.0.CO;2)
- Chou SH, Atlas D, Yeh EN (1986) Turbulence in a convective marine atmospheric boundary layer. *J Atmos Sci* 43(6):547–564. [https://doi.org/10.1175/1520-0469\(1986\)043%3C0547:TIACMA%3E2.0.CO;2](https://doi.org/10.1175/1520-0469(1986)043%3C0547:TIACMA%3E2.0.CO;2)
- Christen A, Rotach MW, Vogt R (2009) The budget of turbulent kinetic energy in the urban roughness sublayer. *Boundary-Layer Meteorol* 131(2):193–222. <https://doi.org/10.1007/s10546-009-9359-5>
- Cuxart J, Morales G, Terradellas E, Yague C (2002) Study of coherent structures and estimation of the pressure transport terms for the nocturnal stable boundary layer. *Boundary-Layer Meteorol* 105:305–328. <https://doi.org/10.1023/A:1019974021434>
- Cuxart J, Holtslag AAM, Beare RJ, Bazile E, Beljaars A, Cheng A, Conangla L, Ek M, Freedman F, Hamdi R, Kerstein A, Kitagawa H, Lenderink G, Lewellen D, Mailhot J, Mauritsen T, Perov V, Schayes G,

- Steenefeld GJ, Svensson G, Taylor P, Weng W, Wunsch S, Xu KM (2006) Single-column model intercomparison for a stably stratified atmospheric boundary layer. *Boundary-Layer Meteorol* 118(2):273–303. <https://doi.org/10.1007/s10546-005-3780-1>
- Deardorff JW (1972) Numerical investigation of neutral and unstable planetary boundary layers. *J Atmos Sci* 29(1):91–115. [https://doi.org/10.1175/1520-0469\(1972\)029%3C0091:NIONAU%3E2.0.CO;2](https://doi.org/10.1175/1520-0469(1972)029%3C0091:NIONAU%3E2.0.CO;2)
- Deardorff JW (1974) Three-dimensional numerical study of the height and mean structure of a heated planetary boundary layer. *Boundary-Layer Meteorol* 7(1):81–106. <https://doi.org/10.1007/BF00224974>
- Deardorff JW, Willis GE (1985) Further results from a laboratory model of the convective planetary boundary layer. *Boundary-Layer Meteorol* 32:205–236. <https://doi.org/10.1007/BF00121880>
- Dias NL, Brutsaert W (1998) Radiative effects on temperature in the stable surface layer. *Boundary-Layer Meteorol* 89:141–159. <https://doi.org/10.1023/A:1001574605472>
- Duynkerke PG (1988) Application of the ϵ - turbulence closure model to the neutral and stable atmospheric boundary layer. *J Atmos Sci* 45(5):865–880. [https://doi.org/10.1175/1520-0469\(1988\)045%3c0865:AOTTCM%3e2.0.CO;2](https://doi.org/10.1175/1520-0469(1988)045%3c0865:AOTTCM%3e2.0.CO;2)
- Edson JB, Fairall CW (1998) Similarity relationships in the marine atmospheric surface layer for terms in the TKE and scalar variance budgets. *J Atmos Sci* 55(13):2311–2328. [https://doi.org/10.1175/1520-0469\(1998\)055%3C2311:SRITMA%3E2.0.CO;2](https://doi.org/10.1175/1520-0469(1998)055%3C2311:SRITMA%3E2.0.CO;2)
- Frenzel P, Vogel CA (1992) The turbulent kinetic energy budget in the atmospheric surface layer: a review and an experimental reexamination in the field. *Boundary-Layer Meteorol* 60:49–76. <https://doi.org/10.1007/BF00122061>
- Garratt JR (1980) Surface influence upon vertical profiles in the atmospheric near-surface layer. *Q J R Meteorol Soc* 106:803–819. <https://doi.org/10.1002/qj.49710645011>
- Han J, Bretherton CS (2019) TKE-based moist Eddy-Diffusivity Mass-Flux (EDMF) parameterization for vertical turbulent mixing. *Weather Forecast* 34(4):869–886. <https://doi.org/10.1175/WAF-D-18-0146.1>
- Iman Gohari SM, Sarkar S (2017) Direct numerical simulation of turbulence collapse and rebirth in stably stratified Ekman flow. *Boundary-Layer Meteorol* 162:401–426. <https://doi.org/10.1007/s10546-016-0206-1>
- Kiely G, Albertson J, Parlange M, Eichinger WE (1996) Convective scaling of the average dissipation rate of temperature variance in the atmospheric surface layer. *Boundary-Layer Meteorol* 77(3):267–284. <https://doi.org/10.1007/BF00123528>
- Kosovic B, Curry JA (2000) A large eddy simulation study of a quasi-steady, stably stratified atmospheric boundary layer. *J Atmos Sci* 57:1052–1068. [https://doi.org/10.1175/1520-0469\(2000\)057%3C1052:ALESSO%3E2.0.CO;2](https://doi.org/10.1175/1520-0469(2000)057%3C1052:ALESSO%3E2.0.CO;2)
- Kurbatskii AF, Kurbatskaya LI (2010) The wind-field structure in a stably stratified atmospheric boundary layer over a rough surface. *Izv Atmos Ocean Phys* 47(3):281–289. <https://doi.org/10.1134/S0001433811030091>
- Lee S, Iman Gohari SM, Sarkar S (2020) Direct numerical simulation of stratified Ekman layers over a periodic rough surface. *J Fluid Mech* 902:A25. <https://doi.org/10.1017/jfm.2020.590>
- LeMone MA (1973) The structure and dynamics of horizontal roll vortices in the planetary boundary layer. *J Atmos Sci* 30(6):1077–1091. [https://doi.org/10.1175/1520-0469\(1973\)030%3C1077:TSADOH%3E2.0.CO;2](https://doi.org/10.1175/1520-0469(1973)030%3C1077:TSADOH%3E2.0.CO;2)
- Lenschow DH (1974) Model of the height variation of the turbulence kinetic energy budget in the unstable planetary boundary layer. *J Atmos Sci* 31(2):465–474. [https://doi.org/10.1175/1520-0469\(1974\)031%3C0465:MOTHVO%3E2.0.CO;2](https://doi.org/10.1175/1520-0469(1974)031%3C0465:MOTHVO%3E2.0.CO;2)
- Lenschow DH, Wyngaard JC, Pennell WT (1980) Mean-field and second-moment budgets in a baroclinic, convective boundary layer. *J Atmos Sci* 37(6):1313–1326. [https://doi.org/10.1175/1520-0469\(1980\)037%3C1313:MFASMB%3E2.0.CO;2](https://doi.org/10.1175/1520-0469(1980)037%3C1313:MFASMB%3E2.0.CO;2)
- Li X, Zimmerman N, Princevac M (2008) Local imbalance of turbulent kinetic energy in the surface layer. *Boundary-Layer Meteorol* 129:115–136. <https://doi.org/10.1007/s10546-008-9304-z>
- Mahrt L, Thomas C, Richardson S, Seaman N, Stauffer D, Zeeman M (2013) Non-stationarity generation of weak turbulence for very stable and weak-wind conditions. *Boundary-Layer Meteorol* 147:179–199. <https://doi.org/10.1007/s10546-012-9782-x>
- Maroneze R, Acevedo OC, Costa FD, Sun J (2019) Simulating the regime transition of the stable boundary layer using different simplified models. *Boundary-Layer Meteorol* 170(2):305–321. <https://doi.org/10.1007/s10546-018-0401-3>
- Mellor GL, Yamada T (1974) A hierarchy of turbulence closure models for planetary boundary layers. *J Atmos Sci* 31(7):1791–1806. [https://doi.org/10.1175/1520-0469\(1974\)031%3C1791:AHOTCM%3E2.0.CO;2](https://doi.org/10.1175/1520-0469(1974)031%3C1791:AHOTCM%3E2.0.CO;2)
- Meyers TP, Baldocchi DD (1991) The budgets of turbulent kinetic energy and Reynolds stress within and above a deciduous forest. *Agric For Meteorol* 53(3):207–222. [https://doi.org/10.1016/0168-1923\(91\)90058-X](https://doi.org/10.1016/0168-1923(91)90058-X)

- Mironov DV, Gryanik VM, Moeng C-H, Olbers DJ, Warncke TH (2000) Vertical turbulence structure and second-moment budgets in convection with rotation: a large-eddy simulation study. *Q J R Meteorol Soc* 126:477–515. <https://doi.org/10.1002/qj.49712656306>
- Moeng C-H, Wyngaard JC (1989) Evaluation of turbulent transport and dissipation closures in second-order modeling. *J Atmos Sci* 46(14):2311–2330. [https://doi.org/10.1175/1520-0469\(1989\)046%3C2311:EOTTAD%3E2.0.CO;2](https://doi.org/10.1175/1520-0469(1989)046%3C2311:EOTTAD%3E2.0.CO;2)
- Moeng C-H, Sullivan PP (1994) A comparison of shear- and buoyancy-driven planetary boundary layer flows. *J Atmos Sci* 51(7):999–1022. [https://doi.org/10.1175/1520-0469\(1994\)051%3C0999:ACOSAB%3E2.0.CO;2](https://doi.org/10.1175/1520-0469(1994)051%3C0999:ACOSAB%3E2.0.CO;2)
- Nakanishi M, Niino H (2009) Development of an improved turbulence closure model for the atmospheric boundary layer. *J Met Soc Japan* 87(5):895–912. <https://doi.org/10.2151/jmsj.87.895>
- Nelson MA, Pardyjak ER, Klein P (2011) Momentum and turbulent kinetic energy budgets within the park avenue street canyon during the joint urban 2003 field campaign. *Boundary-Layer Meteorol* 140(1):143–162. <https://doi.org/10.1007/s10546-011-9610-8>
- Pennell WT, LeMone MA (1974) An experimental study of turbulence structure in the fair-weather trade wind boundary layer. *J Atmos Sci* 31(5):1308–1323. [https://doi.org/10.1175/1520-0469\(1974\)031%3C1308:AESOTS%3E2.0.CO;2](https://doi.org/10.1175/1520-0469(1974)031%3C1308:AESOTS%3E2.0.CO;2)
- Puhales FS, Rizza U, Degrazia GA, Acevedo OC (2013) A simple parameterization for the turbulent kinetic energy transport terms in the convective boundary layer derived from large eddy simulation. *Phys A* 392:583–595. <https://doi.org/10.1016/j.physa.2012.09.028>
- Puhales FS, Demarco G, Martins LGN, Acevedo OC, Degrazia GA, Welter GS, Avelar AC (2015) Estimates of turbulent kinetic energy dissipation rate for a stratified flow in a wind tunnel. *Phys A* 431:175–187. <https://doi.org/10.1016/j.physa.2015.03.008>
- Rubert GC, Roberti DR, Pereira LS, Quadros FL, Velho C, Moraes OLL (2018) Evapotranspiration of the Brazilian Pampa biome: seasonality and influential factors. *Water* 10:1864. <https://doi.org/10.3390/w10121864>
- Salesky ST, Chamecki M, Bou-Zeid E (2017) On the nature of the transition between roll and cellular organization in the convective boundary layer. *Boundary-Layer Meteorol* 163(1):41–68. <https://doi.org/10.1007/s10546-016-0220-3>
- Shah SK, Bou-Zeid E (2014) Direct numerical simulations of turbulent Ekman layers with increasing static stability: modifications to the bulk structure and second-order statistics. *J Fluid Mech* 760:494–539. <https://doi.org/10.1017/jfm.2014.597>
- Smeets CJP, Duynkerke FG, Vugts HF (1998) Turbulence characteristics of the stable boundary layer over a mid-latitude glacier. Part I: a combination of katabatic and large-scale forcing. *Boundary-Layer Meteorol* 87:117–145. <https://doi.org/10.1023/A:100086040609>
- Sjöblom A, Smedman AS (2002) The turbulent kinetic energy budget in the marine atmospheric surface layer. *J Geophys Res Oceans* 107(C10):6–1. <https://doi.org/10.1029/2001JC001016>
- Sreenivasan KR (1995) On the universality of the kolmogorov constant. *Phys Fluids* 7(11):2778–2784. <https://doi.org/10.1063/1.868656>
- Steeneveld G-J, van de Wiel BJH, Holtslag AAM (2006) Modeling the evolution of the atmospheric boundary layer coupled to the land surface for three contrasting nights in CASES-99. *J Atmos Sci* 63(3):920–935. <https://doi.org/10.1175/JAS3654.1>
- Stiperski I, Calaf M, Rotach MW (2019) Scaling, anisotropy, and complexity in near-surface atmospheric turbulence. *J Geophys Res Atmos* 124:1428–1448. <https://doi.org/10.1029/2018JD029383>
- Sun J, Mahrt L, Banta RM, Pichugina YL (2012) Turbulence regimes and turbulence intermittency in the stable boundary layer during “CASES-99.” *J Atmos Sci* 69(1):338–351. <https://doi.org/10.1175/JAS-D-11-082.1>
- Therry G, Lacarrere P (1983) Improving the Eddy kinetic energy model for planetary boundary layer description. *Boundary-Layer Meteorol* 25(1):63–88. <https://doi.org/10.1007/BF00122098>
- van de Wiel BJH, Moene AF, Jonker HJJ, Baas P, Basu S, Donda JMM, Sun J, Holtslag AAM (2012) The minimum wind speed for sustainable turbulence in the nocturnal boundary layer. *J Atmos Sci* 69(11):3116–3127. <https://doi.org/10.1175/JAS-D-12-0107.1>
- van Hooijdonk IGS, Donda JMM, Clercx JH, Bosveld FC, van de Wiel BJH (2015) Shear capacity as prognostic for nocturnal boundary layer regimes. *J Atmos Sci* 72:1518–1532
- Weng W, Taylor PA (2003) On modelling the one-dimensional atmospheric boundary layer. *Boundary-Layer Meteorol* 107:371–400. <https://doi.org/10.1023/A:1022126511654>
- Wilson JD (1988) A second-order closure model for flow through vegetation. *Boundary-Layer Meteorol* 42(4):371–392

- Wyngaard JC, Coté OR (1971) The budgets of turbulent kinetic energy and temperature variance in the atmospheric surface layer. *J Atmos Sci* 28:190–201. [https://doi.org/10.1175/1520-0469\(1971\)028%3C0190:TBOTKE%3E2.0.CO;2](https://doi.org/10.1175/1520-0469(1971)028%3C0190:TBOTKE%3E2.0.CO;2)
- Wyngaard JC, Coté OR, Izumi Y (1971) Local free convection, similarity, and the budgets of shear stress and heat flux. *J Atmos Sci* 28:1171–1182. [https://doi.org/10.1175/1520-0469\(1971\)028%3C1171:LFCSAT%3E2.0.CO;2](https://doi.org/10.1175/1520-0469(1971)028%3C1171:LFCSAT%3E2.0.CO;2)
- Wyngaard JC (1973) On surface layer turbulence, In: Haugen DA (ed.), *Workshop on Micrometeorology*, Amer Meteorol Soc, pp 101–149
- Zhou MY, Lenschow DH, Stankov BB, Kaimal JC, Gaynor JE (1985) Wave and turbulence structure in a shallow baroclinic convective boundary layer and overlying inversion. *J Atmos Sci* 42(1):47–57. [https://doi.org/10.1175/1520-0469\(1985\)042%3C0047:WATSIA%3E2.0.CO;2](https://doi.org/10.1175/1520-0469(1985)042%3C0047:WATSIA%3E2.0.CO;2)

Publisher's Note Springer Nature remains neutral with regard to jurisdictional claims in published maps and institutional affiliations.

Springer Nature or its licensor (e.g. a society or other partner) holds exclusive rights to this article under a publishing agreement with the author(s) or other rightsholder(s); author self-archiving of the accepted manuscript version of this article is solely governed by the terms of such publishing agreement and applicable law.